Controlling Cellular Morphology by Supercritical Carbon Dioxide

Dong Wang, Wei Jiang, Hong Gao, Zhenhua Jiang

Alan G. MacDiarmid Institute, Jilin University, Changchun, People's Republic of China 130012

Received 28 February 2008; accepted 21 August 2008
DOI 10.1002/app.29225
Published online 10 November 2008 in Wiley InterScience (www.interscience.wiley.com).

ABSTRACT: A series of high-performance porous materials, including open-cell and closed-cell foams, were prepared by a two-stage batch foaming process from fluorinated poly(arylene ether)s, and the porous morphology was characterized with scanning electron microscopy. The effects of saturation pressures, saturation temperatures, transfer times, molecular structures, and solvent traces on the cell sizes, cell densities, and bulk densities of porous materials were examined. According to the conclusions, the porous structures could be controlled with cellular sizes between the nanoscale and microscale. All nanoporous materials have dielectric constants in the ultralow-dielectric-constant range (1.4–2.0). The open structures can be prepared by two methods, and there are two kinds of morphologies from the two methods, including foams with small, spotlike openings (diameters between 10 and 100 nm) in the cell walls and bicontinuous nanoporous foams. Another special method for controlling the porous morphology was used here. Films with closed-cell microcellular foams were placed in supercritical carbon dioxide again. The original morphology of the microcellular foam collapsed. The collapsed morphology was also characterized with scanning electron microscopy, and three kinds of cellular morphology were observed. © 2008 Wiley Periodicals, Inc. J Appl Polym Sci 111: 2116–2126, 2009

Key words: amorphous; high performance polymers; macroporous polymers; morphology; poly(ether ketones)

INTRODUCTION

With unique properties, microcellular foams have encouraged a number of innovative applications in fields such as packaging materials, insulation, filtration membranes, sports equipment, automobiles, and aircraft parts. Supercritical carbon dioxide (SC-CO_2) is of significant interest as an environmentally innocuous physical blowing agent that is used to introduce microscopic cells into polymers.[1–7] The aforementioned techniques have been used to investigate the foaming behavior of amorphous and semicrystalline glassy polymers such as polyimides,[8] poly(ethylene terephthalate),[9] poly(methyl methacrylate),[1] polystyrene,[2–4] polycarbonate,[6,10] and polysulfone.[7]

Within the next few years, high-performance chips containing as many as billions of transistors on a single chip will be produced. The search is now on for materials that can replace silicon dioxide as the insulator in these future devices.[11] Nonpolar polymers allow us to conquer the low-dielectric-constant region; nonetheless, only a few polymers meet the mechanical strength and temperature requirements. In the quest to lower the permittivity of polymers down to ultralow-dielectric-constant values, several research groups are exploring the incorporation of nanosized air cells.[12–14] Conventional SC-CO_2 processes, in which CO_2 is introduced into polymeric monoliths and depressurized quickly to foam, have produced few closed nanoscopic cells (nanocells), that is, cells less than 100 nm in diameter, in polymers. Krause et al.'s[8] batch process invokes the foaming created by the evaporation of dissolved SC-CO_2. A series of ultralow-dielectric-constant nanocell materials were made.

Open-cell, microcellular, thermoplastic foam offers a range of properties well suited for many microporous material applications. The open-cell structure allows particles and fluids to flow through the material, resulting in a product that can be used as a filter or membrane. In addition, the thermoplastic base material offers many desirable properties, such as high strain to failure, high fracture toughness, low thermal conductivity, low electrical conductivity, and good chemical resistance. These properties offer many advantages over other microporous materials.[15] Closed-cell foams have been prepared in many works,[1–9,16] but open-cell foams are few.[8,15,17–21] Open-cell polysulfone was described by Krause and coworkers,[17,18] and the solvent traces are pore openers. Bicontinuous nanoporous polymers were also described by Krause and coworkers,[19,20] and the open-cell region around the gas concentration was found.

Correspondence to: Z. Jiang (jiangzhenhua@jlu.edu.cn).

© 2008 Wiley Periodicals, Inc.

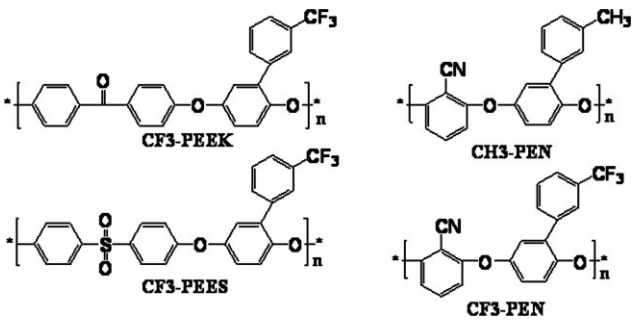

Figure 1 Structures of PAEs.

In this article, the processing conditions necessary for closed-cell and open-cell foams are verified. We also study the nanoporous foaming process of a series of amorphous, high glass-transition temperature (T_g), fluorinated poly(aryl ether)s as low-dielectric-constant materials. The novel exploration of the collapse of the microcellular morphology under supercritical conditions is another main purpose.

EXPERIMENTAL

Four stiff and aromatic poly(aryl ether)s with different pendant groups were synthesized in our laboratory (see Fig. 1).[22–24] Here, they were selected as the matrix for their low intrinsic dielectric constant and thermal stability. The molecular weights, polydispersities, T_g values, and mass densities of the prepared polymer films are summarized in Table I. CO_2 with a specified purity better than 99.99% was obtained from Beijing Analytical Gas Factory (Beijing, China).

A solution of poly(arylene ether)s (PAEs) was prepared by the dissolution of 20 wt % polymers in *N*-methylpyrrolidone (NMP). Thin films around 150 μm thick were formed by solution casting on a glass plate. The cast films were dried in a nitrogen atmosphere at 80°C for 24 h. Subsequently, the homogeneous dense films were removed from the glass plate with the help of a small amount of water and further dried *in vacuo* at 80°C for several weeks to remove the last traces of the solvents. These films were analyzed with elemental analysis (N) to determine remaining NMP traces. The remaining solvent traces were all less than 0.03 wt %.

The foaming experiments were performed in a two-stage batch process. In the first stage, the films were saturated in a pressure vessel with SC-CO_2 maintained at the setting pressure and temperature for 2 h. The pressure was then quickly released, and the samples were removed from the vessel and kept in air for the setting time before foaming. In the second stage, the supersaturated samples were foamed for a predetermined period of time in an oil bath with selected foaming temperatures for 60 s, and then the samples were quenched in ice water.

The process of preparing collapsed samples was similar to the first stage previously described. The aforementioned foams were saturated in a pressure vessel with CO_2 gas maintained at the saturation pressure of 20 MPa and at the saturation temperature of 20 or 40°C for 10 min, 2 h, or 6 h. The pressure was then quickly released, and the samples were removed from the vessel.

The element nitrogen was analyzed with a Vario EL elemental analysis instrument (Hanau, Germany). The microcellular morphologies of the foamed samples were investigated with a Shimadzu SSX-550 scanning electron microscope (SEM) (Kyoto, Japan). The samples were freeze-fractured in liquid nitrogen and sputter-coated with gold at an argon pressure of 0.1 Torr for 10 min at a current of 15 mA. The dielectric constants were measured with a Hewlett–Packard 4192A LF at 25°C and 1 kHz (CA). The cell diameter (D), cell density [number of bubbles per cubic centimeter of the foam (N_f)], porosity [volume occupied by the voids in one cubic centimeter of the foam (V_f)], and nucleated density [number of bubbles nucleated per cubic centimeter of the original unfoamed polymer (N_0)] were determined from scanning electron microscopy (SEM) micrographs with a procedure described previously by Kumar and Weller.[5]

RESULTS AND DISCUSSION

The influences of the foaming conditions on the porous morphologies are very complex, and it seems that there is no simple answer about how the cellular structure changes with them. It depends on the specific foaming system because nearly all the physical properties, such as the viscosity, surface tension, solubility, and diffusivity, are sensitive functions of the foaming conditions. The final changes in the cell size, cell density, and cell morphology are

TABLE I
PAE Polymer Film Properties

Sample	M_n (kg/mol)	M_w (kg/mol)	M_w/M_n	T_g (°C)	Density (g/cm^3)
CF3-PEEK	42,500	63,300	1.49	136	1.32
CF3-PES	50,200	88,400	1.76	167	1.28
CF3-PEN	32,700	39,500	1.21	151	1.31
CH3-PEN	38,600	47,600	1.24	168	1.20

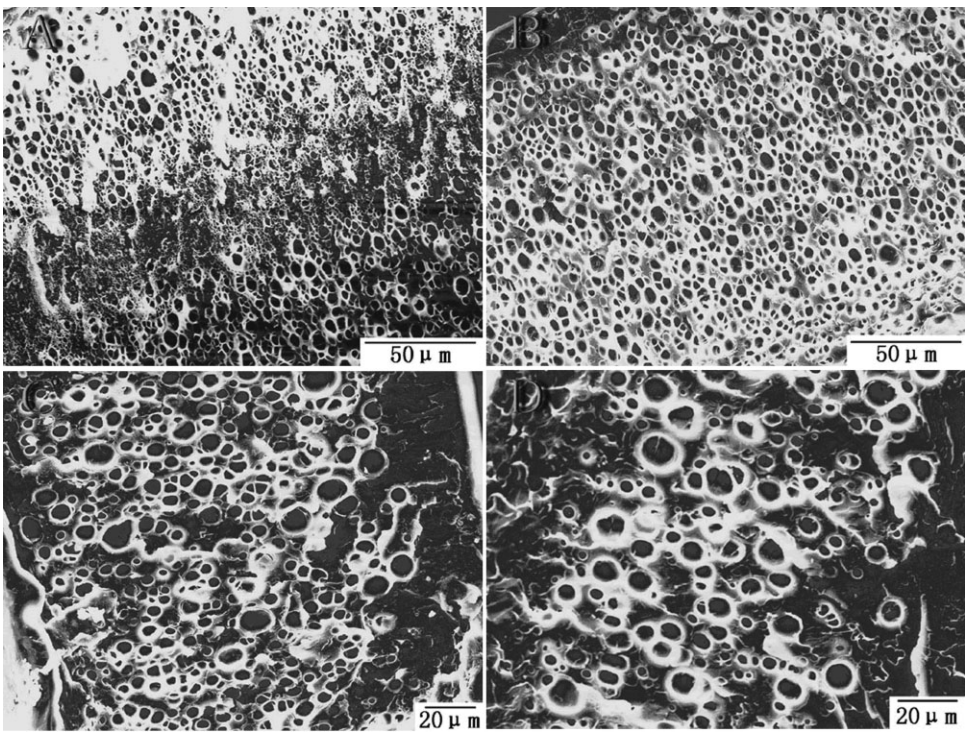

Figure 2 SEM images of foaming CF3-PEEK films with different transfer times: (A) 30, (B) 60, (C) 120, and (D) 300 s (foaming temperature = 80°C, foaming time = 60 s).

results of the comprehensive interactions of all these parameters.

Closed foams

Although simplified in many aspects, this rendition of the microcellular morphology serves as a basis for elucidating various fundamental features that pertain to the emergence of the morphology of polymer foams. However, for the purpose of demonstration, the simplest case of closed microcellular morphology is considered first.

Because foaming can take place only above the T_g value of the polymer/gas mixture, the foaming temperature is an important parameter for controlling the foam morphology. The influence of the foaming temperature on the cellular morphology is very complex, and some results have been described in the previous work.[25] To investigate the influence of the foaming temperature on the cellular morphology under the applied conditions, CF3-PEEK samples were foamed at 80, 100, 120, or 140°C. The microcellular morphologies of the foamed samples were investigated with SEM, and the results are shown in Figures 2–5. D, N_f, V_f, and N_0 were calculated and are summarized in Table II. D, N_f, V_f, and N_0 increased with the foaming temperature increasing. The increment of D was due to the reduction of the viscosity. The viscosity of CF3-PEEK decreased with increasing temperature, and the physical constraint that controlled the cellular growth decreased. The increment of N_f and N_0 was due to the increment of the nucleation rate. This is the reason that the nucleation rate increases with the foaming temperature increasing (according to the classical nucleation theory). The increment of V_f was due to both the increment of the nucleation rate and the reduction of the viscosity at the same time.

The transfer time can be used as a main variable to control the void dimensions. During the transfer of the gas-saturated polymer from the pressure vessel to the heating bath, CO_2 diffusion from the polymers occurs. This process will lower the CO_2 concentration. The results with different transfer times are shown in Figures 2–5. Lowering the transfer time to 30 s caused a significant increase in the CO_2 concentration. It can be observed from Table II that with an increase in the transfer time, D increased and N_f, V_f, and N_0 decreased at the same time. In addition, homogeneous nucleation theory predicts that, as the gas concentration increases, more cells will be nucleated within a given volume. This will lead to the smallest cell sizes overall.

Opened foams

For CF3-PEEK, thin-wall cells were observed when the foaming temperature was 140°C. The cellular walls were flattened to form thin films of the material when they impinged on one another as the

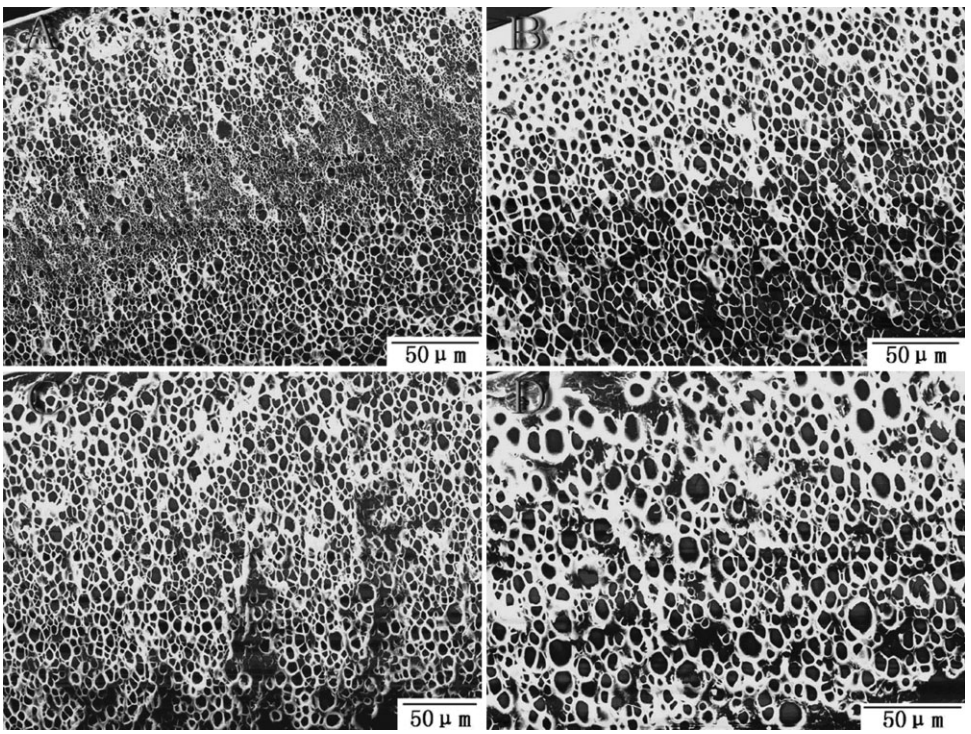

Figure 3 SEM images of foaming CF3-PEEK films with different transfer times: (A) 30, (B) 60, (C) 120, and (D) 300 s (foaming temperature = 100°C, foaming time = 60 s).

bubbles were growing. When there was NMP as a residual solvent in the films, small, spotlike openings (diameters between 10 and 100 nm) in the cell walls were observed. The morphology with residual solvent is shown in Figure 6(A–C). For comparison, the morphology with only traces of NMP (<0.02 wt %)

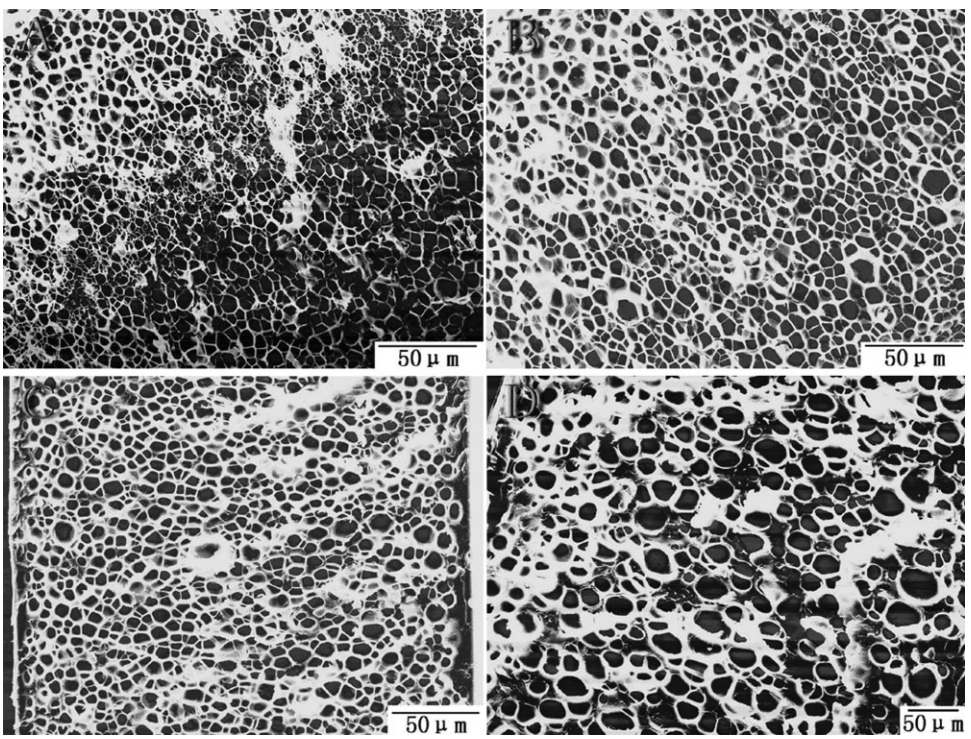

Figure 4 SEM images of foaming CF3-PEEK films with different transfer times: (A) 30, (B) 60, (C) 120, and (D) 300 s (foaming temperature = 120°C, foaming time = 60 s).

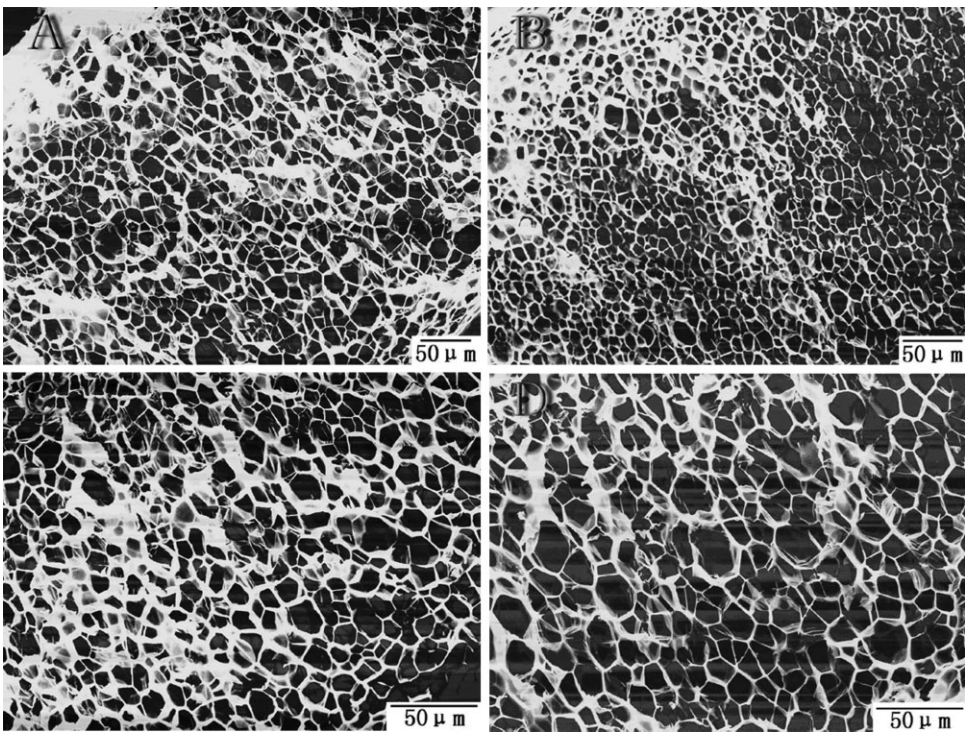

Figure 5 SEM images of foaming CF3-PEEK films with different transfer times: (A) 30, (B) 40, (C) 80, and (D) 600 s (foaming temperature = 140°C, foaming time = 60 s).

in the polymer matrix is also shown in Figure 6(D). Both samples [Fig. 6(A,D)] were saturated with 20 MPa of CO_2 at 20°C and subsequently foamed at 140°C for 5 s. Figure 6(A) clearly shows small holes in the cell walls. The open-cell structures were not found in the low-foaming-temperature region, whether or not the concentration of NMP (the residual solvent) in the structure was more than 0.02 wt %. Two factors should be taken into consideration: (1) the impingement of bubbles and (2) the residual solvent. The development mechanism for an open-cell structure indicates that two stages exist: bubble growth to impingement and then cell wall thinning to rupture.

The structural transition of foams prepared above the critical value of the CO_2 concentration reported previously[17] leads to bicontinuous nanoporous films. Figure 7 shows a bicontinuous CF3-PEEK foam prepared at a foaming temperature of 120°C for 60 s. For an opened foam, the critical CO_2 concentration is necessary. The permeability of the polymer itself is large, so lowering the transfer time causes a significant increase in the CO_2 concentration. The method that causes the high CO_2 concentration has been mentioned previously. Another method is lowering the saturation temperature, which can produce an increase in the solubility of CO_2 in the films. These foaming conditions are beneficial for preparing bicontinuous nanoporous samples.

Nanoporous foams

Only nanoporous structures with cellular sizes below 100 nm have the potential for applications in multilayer microelectronic devices. In the previous work[25] and as previously discussed, several variables that could influence the foam morphology were optimized and fixed to elaborate the effects of

TABLE II
Statistics of CF3-PEEK Cellular Morphology

Foaming temperature (°C)	Transfer time (s)	D (μm)	V_f	N_f (10^9)	N_0 (10^9)
80	30	—	—	—	—
	60	5	0.32	4.88	7.16
	120	5.79	0.31	3	4.37
	300	7.7	0.27	1.13	1.54
100	30	—	—	—	—
	60	5.6	0.58	6.3	15
	120	5.8	0.54	5.3	11.6
	300	6.5	0.5	3.5	7.1
120	30	—	—	—	—
	60	7	0.74	4.1	16
	120	7.2	0.64	3.3	11.6
	300	8.2	0.5	1.74	3.5
140	30	15	0.634	0.36	0.98
	45	10	0.77	1.47	6.44
	75	13	0.83	0.7	4.6
	600	15.4	0.85	0.45	3

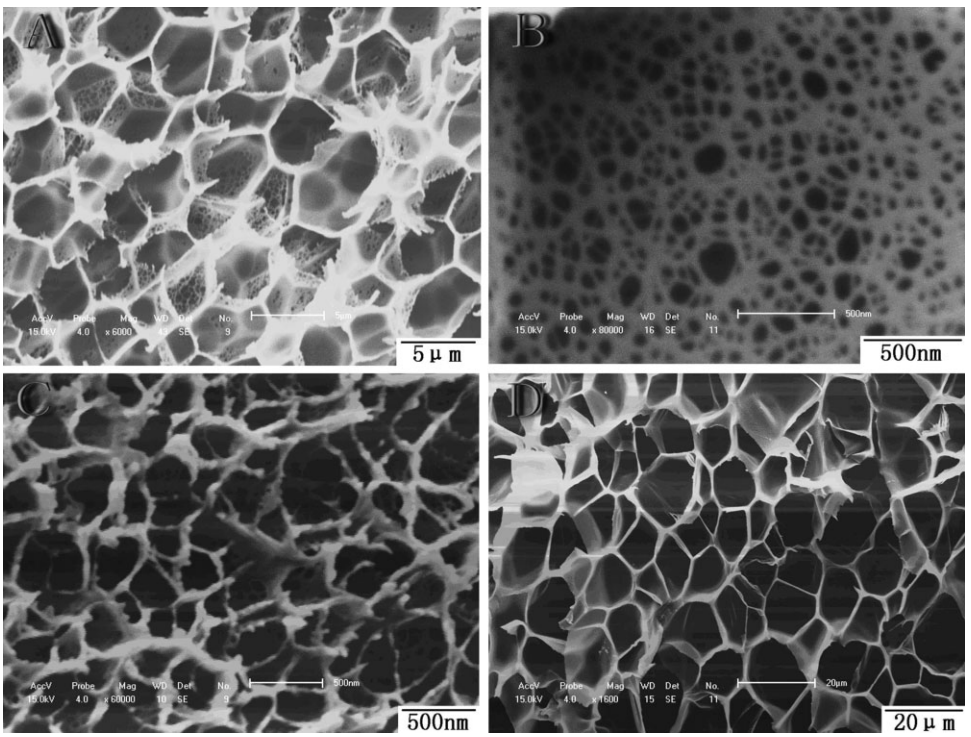

Figure 6 SEM images of CF3-PEEK opened foam with residual solvent: (A) a saturation pressure of 5 MPa, a foaming temperature of 140°C, and a transfer time of 20; (B) a magnification of image A; (C) a saturation pressure of 10 MPa, a foaming temperature of 140°C, and a transfer time of 10; and (D) a saturation pressure of 5 MPa, a foaming temperature of 140°C, and a transfer time of 20 s without residual solvent.

changing just one of these variables on the microcellular foam morphology. Figure 8 shows the smallest cellular morphology of every PAE with different pendant groups. The porous PAE films displayed a cellular morphology with cell dimensions between 30 and 500 nm. The cellular diameters of PAEs with different pendant groups were 410, 900, 65, and 30 nm for CF3-PEEK, CH3-PEN, CF3-PES, and CF3-PEN, respectively. The density reduction of the constrained foams was limited to approximately 0.5 g/cm^3. The nanoporosity was obtained through the control of the foaming conditions and the structures of the polymers.

Effect of transfer times on cells

During the transfer of the gas-saturated polymer from the pressure vessel to the heating bath, CO_2 diffusion from the polymer occurs. This process lowers the CO_2 concentration. Lowering the transfer time to 20 s causes a significant increase in the CO_2 concentration.[26] The large influence of the CO_2 concentration becomes apparent when we compare the SEM micrograph with one shown in the previous work[25] (transfer time = 40 s): nanofoam morphologies emerge when the transfer time is lowered. According to the previous discussion about homogeneous nucleation theory, as the gas concentration increases, there will be smaller cell sizes overall.

Effect of foaming temperatures on cells

According to classical nucleation theory, the nucleation rate increases with increasing foaming temperature. Increasing the temperature decreases the viscosity of the substrate material, causing the retractive force restricting cell growth to decrease and the diffusivity of CO_2 within the substrate to increase. The increment of the nucleation rate is

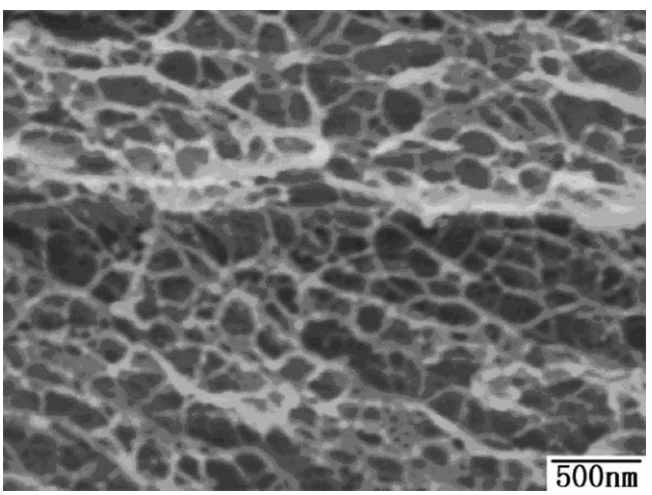

Figure 7 SEM image of CF3-PEEK opened foam without residual solvent (saturation pressure = 30 MPa, foaming temperature = 130°C, transfer time = 10 s).

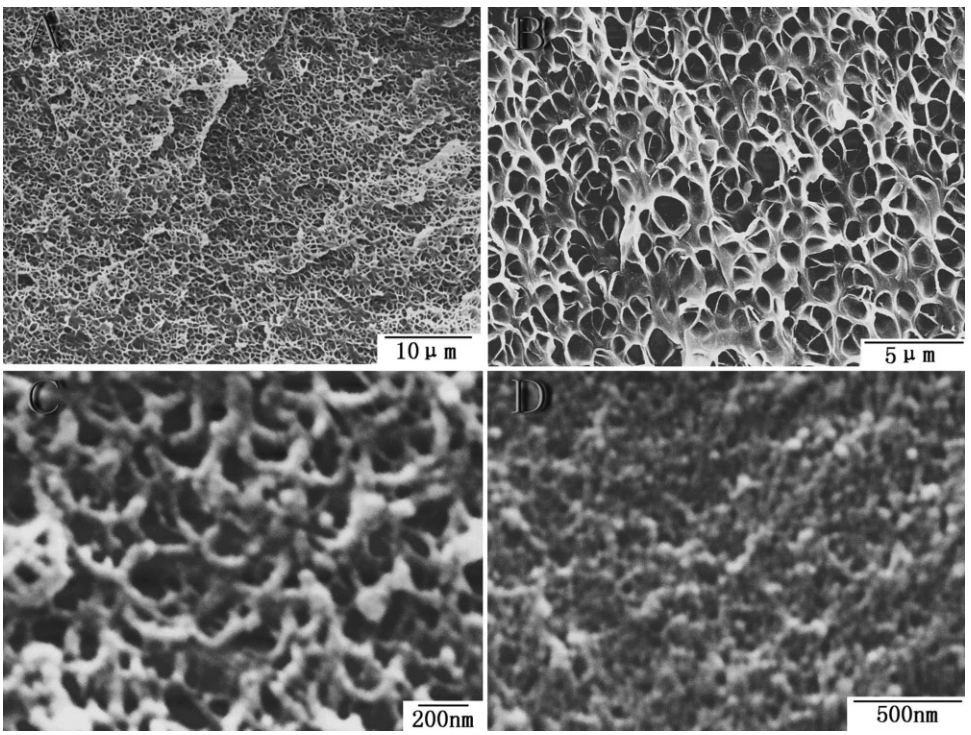

Figure 8 Cellular morphology of PAEs with different pendants and foaming conditions: (A) CF3-PEEK at 100°C, (B) CH3-PEN at 140°C, (C) CF3-PES at 140°C, and (D) CF3-PEN at 140°C.

beneficial for preparing smaller cells, and the reduction of the viscosity is reversed.

Effect of polymer structures on cells

The polymer structures also affect the cellular morphology directly. Increasing the nucleation rate and viscosity simultaneously is beneficial for a smaller cell size. For improving both characteristics, the polymer structure must be designed, and the polymer must have a high T_g value for a high foaming temperature, bulky pendant groups for a high gas concentration, and strong stiffness for restricting cell growth. The relations between these factors and the polymer structure are discussed here in detail:

1. High gas concentration: According to the previous work,[26] the bulky pendant groups and higher content of fluorine are of great importance to the higher gas content. From this point, CF3-PES, CF3-PEEK, and CF3-PEN will adsorb more gases, having higher nucleation rates and smaller cellular sizes.
2. High T_g: A higher T_g value is important for a higher foaming temperature. From this point, CF3-PES, CH3-PEN, and CF3-PEN will have a higher T_g value and a smaller cellular size.
3. Strong stiffness: In the previous set of experiments, the constrained foams had smaller cells than their unconstrained counterparts. In a comparison with the corresponding polymers containing ketone, sulfone, or other groups, poly (arylene ether nitrile) exhibited excellent performance because of the highly rigid nitrile groups introduced into the structures of poly (aryl ether)s. The stiffness was attributable to dipole–dipole interactions of nitrile. From this point, CH3-PEN and CF3-PEN will have higher stiffness and a smaller cellular size.

In summary, CF3-PEN has a higher gas content, T_g, and stiffness than the others, and it must have the smallest cellular size. From Figure 8, it can be proved that the results for the cellular sizes are the same as our predictions about the smallest cellular sizes.

If the cellular sizes are less than 100 nm, the foams can be used in low-dielectric-constant materials. Some dielectric constants of these foams are shown in Figure 9. For a comparison of PAEs of various porosities, we can therefore restrict the discussion to values of the dielectric constant at 1 kHz and 25°C. As anticipated, all foams (samples) showed a considerable reduction in the dielectric constant. It dropped to 1.43 for the foamed materials. Interestingly, this was already below the ultralow-dielectric-constant limit.

The drop in the dielectric constant with the void fraction shows a trend, which indeed follows the prediction for an ideal layer or series model.[8]

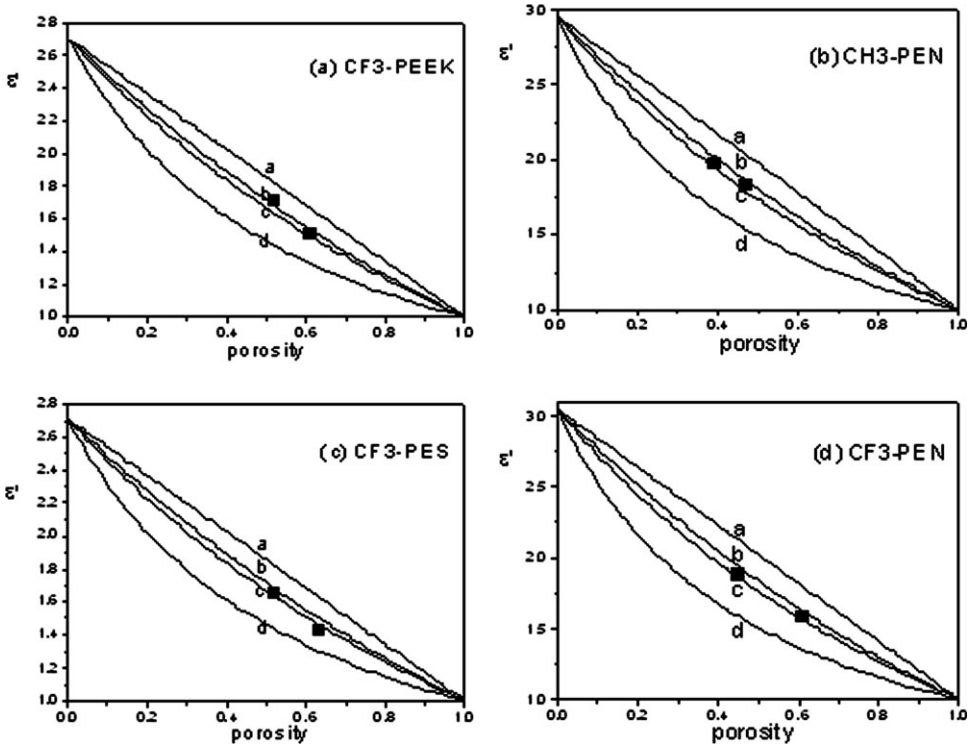

Figure 9 Relation between the porosity and permittivity (ε′): (a) parallel model, upper limit; (b) Maxwell–Garnett model for spheres; (c) Looyenga–Landau–Lifshitz model for spheres; and (d) series model, lower limit.

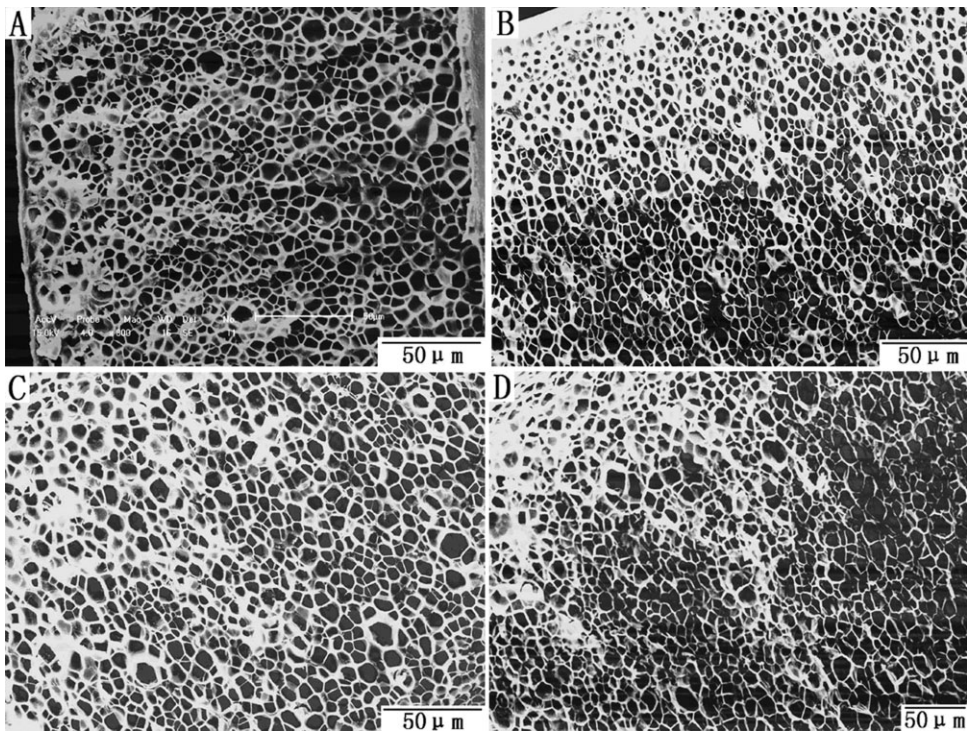

Figure 10 Typical SEM micrographs of CF3-PEEK microcellular foams: (A) a saturation temperature of 40°C, a foaming temperature of 120°C, and a transfer time of 40 s; (B) a saturation temperature of 20°C, a foaming temperature of 100°C, and a transfer time of 60 s; (C) a saturation temperature of 20°C, a foaming temperature of 120°C, and a transfer time of 60 s; (D) a saturation temperature of 20°C, a foaming temperature of 140°C, and a transfer time of 60 s (saturation pressure = 20 MPa, saturation time = 2 h, foaming time = 60 s).

TABLE III
Statistics for the Cellular Morphology of the Original CF3-PEEK Samples

	Sample			
	A	B	C	D
D (μm)	5.4	6	5.6	8.7
N_0 (10^9)	5.65	7.74	9.32	6.45
N_f (10^9)	3.92	4.13	5.02	1.47
V_f	0.369	0.467	0.461	0.771

Clearly, a far more pronounced decrease in the dielectric constant is observed for foams than for amorphous poly(aryl ether)s; the dielectric constant at $v_f = 0.4$ is already as low as 2.0 despite the high intrinsic dielectric constant of 3.0. According to Figure 9, the results of the experiments are in accordance with the predictions.

Cellular collapse

Many foaming conditions can influence the cellular morphology, as reported in the previous work.[25] Some preparation conditions were selected to obtain a series of CF3-PEEK foams for the next collapsed experiment. Four microcellular foams were prepared under different experimental conditions. The microcellular morphologies are shown in Figure 10, and D, N_f, V_f, and N_0 are summarized in Table III. According to the morphology in Figure 10, the foams had different cell-wall thicknesses and microcellular morphologies.

In the previous work,[25] it was demonstrated that the thermal and tensile history could affect the cellular morphology in the dynamic mechanical analysis testing and the controlling temperature tensile test. Here we consider that SC-CO_2 can provide a particular condition that will change the microcellular

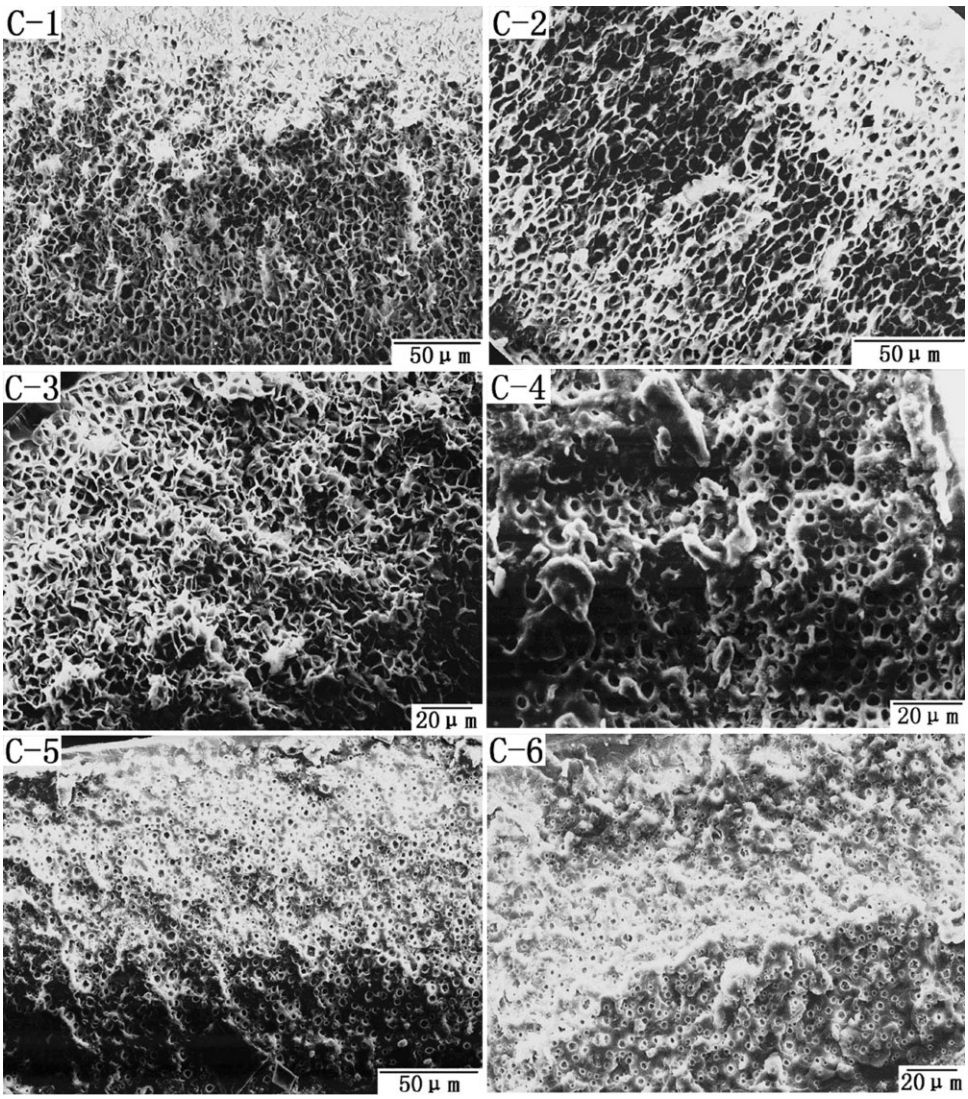

Figure 11 Typical SEM micrographs of CF3-PEEK collapsed microcellular foams in SC-CO_2.

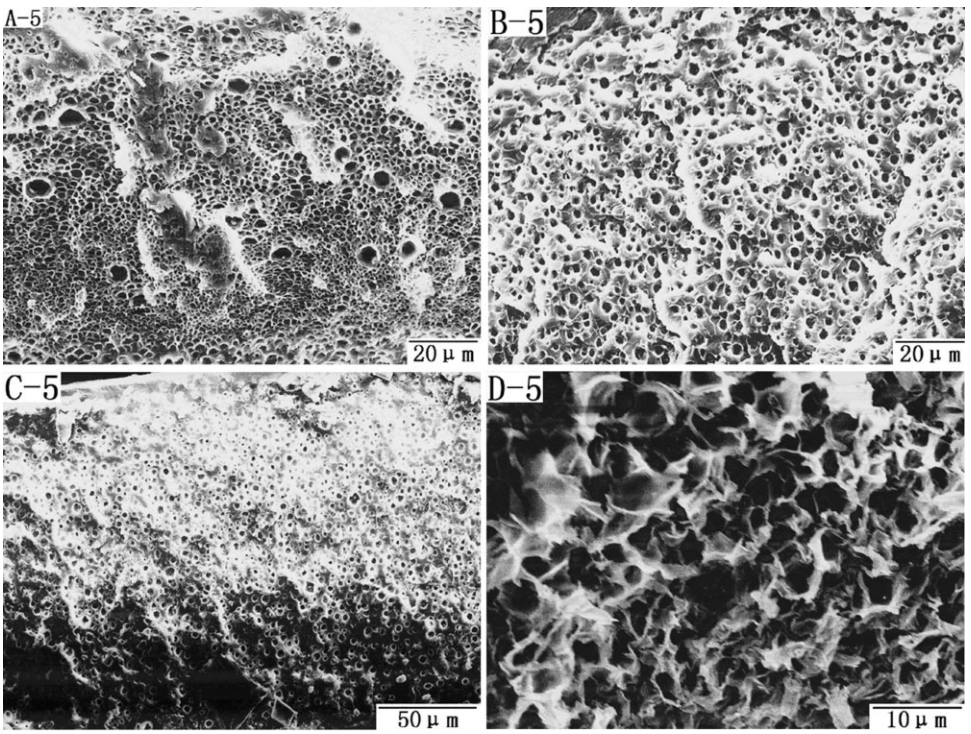

Figure 12 Typical SEM micrographs of CF3-PEEK collapsed microcellular foams in SC-CO_2.

morphology, and the change is related to the dissolution of CO_2 in the films. To validate the idea, microcellular CF3-PEEK foams were placed under SC-CO_2 conditions again. The original morphology of the microcellular foam was changed drastically. The collapsed morphology was also characterized with SEM, and the results are shown in Figure 11 and 12. The species of collapsed morphology under different conditions are summarized in Table IV, and D, N_f, V_f, and N_0 are summarized in Table V. The symbols of the samples include a letter (A–D) to indicate the origin and a number (1–6) to indicate the saturation condition. Three kinds of cellular morphology were observed under the different preparation conditions: irregular (e.g., A5), uniform (e.g., C5), and compressed (e.g., C1). The influences of the saturation temperatures, saturation times, and original microcellular morphologies on the collapsed morphologies are discussed next.

The phenomena are related to the dissolution of CO_2 in the films. During gas dissolution, the gas molecules occupy the free volume of the polymer. As the gas concentration increases, the polymer begins to swell, and this corresponds to an increase in the mean spacing between the polymer chain segments. Once a critical gas concentration is reached, the mean distance between the polymer chain segments reaches a critical value. Above this critical spacing, chain segments have sufficient energy and mobility for molecular relaxation.

The influence of the saturation temperature on the collapsed morphologies can be observed in Figure 11. Comparing C1 to C2, C3 to C4, and C5 to C6, we can see that the cellular shapes in C1 and C3 are

TABLE IV
Species of CF3-PEEK Collapsed Morphology

	Condition[b]					
Sample[a]	10 min (1)[c]	120 min (2)[c]	720 min (3)[c]	10 min (4)[d]	120 min (5)[d]	720 min (6)[d]
A	I	C	C	I	I	C
B	C	C	C	C	U	U
C	C	C	C	U	U	U
D	C	C	C	I	C	C

C = compressed; I = irregular; U = uniform.
[a] The original samples in Figure 2.
[b] Saturation conditions in SC-CO_2.
[c] 20°C.
[d] 40°C.

TABLE V
Statistics for the Cellular Morphology of CF3-PEEK Uniform Samples

	Sample				
	B5	B6	C4	C5	C6
D (μm)	2.2	2.1	3.5	3.1	1.77
N_f (10^9)	27.16	6.33	8.6	8.7	8.7
V_f	0.151	0.031	0.193	0.136	0.025

changed and compressed. Moreover, the cellular shapes in C2, C4, and C6 are also circular, but the thickness of the cell wall, cellular sizes, and cellular densities are changed. When the saturation temperature is 20°C, the content of CO_2 is higher, but the mobility of the chain segments is lower. The chain segments do not have sufficient energy to relax, so the change in the morphology should be small. However, a compressed morphology is observed. The phenomenon could be due to the ultralow temperature, which is brought by the quickly released pressure in the vessel. The gases in the cells are cooled rapidly, and the air pressure in the cells decreases rapidly. The difference in the pressures inside and outside the cells is the driving force for the cellular collapse. When the saturation temperature is 40°C, the chain segments have sufficient energy to relax, so cell coalescence can be observed. The statistical results summarized in Table V indicate that D and V_f decrease with increasing saturation temperatures.

The influences of the saturation times on the collapsed morphologies can be observed in Figure 11. Comparing C2, C4, and C6, we can see that D, N_f, and V_f decrease with increasing saturation times.

The influence of the original microcellular morphologies on the collapsed morphologies can be observed in Figure 12. When the foaming temperature was 140°C, the cellular wall of the microcellular foam was thin. When this sample was saturated in SC-CO_2, the distortion was dramatic. The shapes of the films were destroyed. The microcellular morphology can be seen in Figure 12(D5). When the foaming temperature was 100 or 120°C, the cellular wall of the microcellular foam was thick. When this sample was saturated in SC-CO_2, the shapes of the films were still cuboid, but the sizes of the samples were reduced.

CONCLUSIONS

We have presented a novel, versatile approach to the production of polymer films of various porous morphologies. First, closed microcellular samples were successfully prepared from high-performance thermoplastics with a two-stage batch foaming process. Second, open structures were prepared by two methods, and two kinds of morphologies were observed: (1) if there was NMP as a residual solvent in the films, the morphology included small, spotlike openings in the cell walls, and (2) if the CO_2 concentration was increased, the morphology was bicontinuous and nanoporous. Third, depending on T_g of the aromatic poly(aryl ether)s, mechanically and thermally stable films were formed with a nanoporosity of about 40% and dielectric constants below 2.0. Lastly, the microcellular foams were placed in SC-CO_2 again. The original microcellular morphology was collapsed, and three kinds of collapsed morphology were observed. This method can be used to prepare foams with thick cellular walls and small cellular sizes.

References

1. Mizumoto, T.; Sugimura, N.; Moritani, M. Macromolecules 2001, 33, 6757.
2. Stafford, C. M.; Russel, T. P.; McCarthy, T. J. Macromolecules 1999, 32, 7610.
3. Arora, K. A.; Lesser, A. J.; McCarthy, T. J. Macromolecules 1998, 31, 4614.
4. Sumarno; Sato, Y.; Takishima, S.; Masuoka, H. J Appl Polym Sci 2000, 77, 2383.
5. Kumar, V.; Weller, J. E. J Eng Ind 1994, 116, 413.
6. Liang, M. T.; Wang, C. M. Ind Eng Chem Res 2000, 39, 4622.
7. Krause, B.; Mettinkhof, R.; van der Vegt, N. F. A.; Wessling, M. Macromolecules 2001, 34, 874.
8. Krause, B.; Koops, G. H.; van der Vegt, N. F. A.; Wessling, M.; Wübbenhorst, M.; van Turnhout, J. Adv Mater 2002, 14, 1041.
9. Guan, R.; Wang, B. Q.; Lu, D. P. J Appl Polym Sci 2003, 88, 1956.
10. Ito, Y.; Yamashita, M.; Okamoto, M. Macromol Mater Eng 2006, 291, 773.
11. Miller, R. D. Science 1999, 286, 421.
12. Pai, R. A.; Humayun, R.; Schulberg, M. T.; Sengupta, A.; Sun, J. N.; Watkins, J. J. Science 2004, 303, 507.
13. Wang, W. C.; Vora, R. H.; Kang, E. T.; Neoh, K. C.; Ong, C. K.; Chen, L. F. Adv Mater 2004, 16, 54.
14. Li, L.; Yokoyama, H.; Nemoto, T.; Sugiyama, K. Adv Mater 2004, 16, 1226.
15. Rodeheaver, B. A.; Coltion, J. S. Polym Eng Sci 2001, 41, 380.
16. Arora, K. A.; Lesser, A. J.; McCarthy, T. J Polym Eng Sci 1998, 38, 2055.
17. Krause, B.; van der Vegt, N. F. A.; Wessling, M. Desalination 2002, 144, 5.
18. Krause, B.; Boerrigter, M. E.; van der Vegt, N. F. A.; Strathmann, H.; Wessling, M. J Membr Sci 2001, 187, 181.
19. Krause, B.; Sijbesma, H. J. P.; Münüklü, P.; van der Vegt, N. F. A.; Wessling, M. Macromolecules 2001, 34, 8792.
20. Krause, B.; Diekmann, K.; van der Vegt, N. F. A.; Wessling, M. Macromolecules 2002, 35, 1738.
21. Despois, J. F.; Mortensen, A. Acta Mater 2005, 53, 1381.
22. Liu, B. J.; Hu, W.; Rao, X. H.; Wang, G. B.; Jiang, Z. H.; Wu, Z. W.; Matsumoto, T. Polym Bull 2004, 52, 235.
23. Liu, B. J.; Hu, W.; Chen, C. H.; Jiang, Z. H.; Zhang, W. J.; Wu, Z. W. Polym Adv Technol 2003, 14, 221.
24. Liu, B. J.; Hu, W.; Zhao, S. A.; Chen, C. H.; Wu, Z. W.; Matsumoto, T. Polym J 2003, 35, 628.
25. Wang, D.; Jiang, W.; Gao, H.; Jiang, Z. H. J Polym Sci Part B: Polym Phys 2007, 45, 173.
26. Wang, D.; Jiang, W.; Gao, H.; Jiang, Z. H. J Membr Sci 2006, 281, 203.